catalysts

MDPI

Article

In Situ Growth of $NiSe_2$-$MoSe_2$ Heterostructures on Graphene Nanosheets as High-Performance Electrocatalyst for Hydrogen Evolution Reaction

Tianjun Dai [1], Zhangyu Zhou [1,*], Han Xiao [2], Yingchun Luo [2], Yongchi Xu [1] and Xinqiang Wang [3,*]

[1] School of Electronic and Communication Engineering, Guiyang University, Guiyang 550005, China; dz0015@gyu.cn (T.D.); yongchixu@126.com (Y.X.)
[2] School of Chemical Engineering, Guizhou Minzu University, Guiyang 550025, China; hanx@gzmu.edu.cn (H.X.); yingchunluo_gzmu@163.com (Y.L.)
[3] Institute of Science and Technology for New Energy, Xi'an Technological University, Xi'an 710021, China
* Correspondence: zhouzhangyu@gyu.edu.cn (Z.Z.); wangxinqiang@xatu.edu.cn (X.W.)

Abstract: Developing highly efficient and stable electrocatalysts for hydrogen evolution reaction (HER) is regarded as a crucial way to reduce energy loss in water splitting. Herein, $NiSe_2$/$MoSe_2$ heterostructures grown on graphene nanosheets ($NiSe_2$-$MoSe_2$ HTs/G) have been in situ synthesized by a simple hydrothermal reaction. As an electrocatalyst for HER, $NiSe_2$-$MoSe_2$ HTs/G delivers superior performance with a low Tafel slope of 65 mV dec^{-1}, a small overpotential of 144 mV at 10 mA cm^{-2}, and long-term stability up to 24 h. The superior performance for HER can be mainly ascribed to the synergistic effects of $NiSe_2$-$MoSe_2$ heterostructures, which can facilitate the rapid electron transfer from the electrode to the exposed $MoSe_2$ edges to take part in the HER reaction, thus boosting the HER kinetics. Moreover, the graphene matrix with high conductivity can not only improve the overall conductivity of the composite but also greatly increase the exposed active sites, therefore further promoting the HER performance. This study provides a simple route for fabricating bimetallic selenides-based heterostructures on graphene as an efficient and stable electrocatalyst for HER.

Keywords: $NiSe_2$/$MoSe_2$ heterostructures; synergistic effect; electrocatalyst; HER

Citation: Dai, T.; Zhou, Z.; Xiao, H.; Luo, Y.; Xu, Y.; Wang, X. In Situ Growth of $NiSe_2$-$MoSe_2$ Heterostructures on Graphene Nanosheets as High-Performance Electrocatalyst for Hydrogen Evolution Reaction. *Catalysts* **2022**, *12*, 701. https://doi.org/10.3390/catal12070701

Academic Editors: Carlo Santoro and Nicolas Alonso-Vante

Received: 14 April 2022
Accepted: 10 June 2022
Published: 27 June 2022

1. Introduction

The excessive combustion of fossil fuels in our daily life has brought about severe environmental problems and energy crises [1]. As we all know, hydrogen, a renewable energy source, has been considered a promising candidate to replace natural fossil fuels due to its clean combustion products and high energy density [2–4]. Electrochemical water splitting has been regarded as an efficient strategy to produce hydrogen [5]. However, the high overpotentials on the electrodes severely increase the power consumption and cost in the real electrocatalytic process [6]. Platinum (Pt), a commercial catalyst, has been identified as the most efficient electrocatalyst for the HER [7]. However, its extreme scarcity results in high costs, which limits the commercialization. Hence, highly efficient non-noble metal catalysts must be developed to reduce the overpotential in the HER, aiming to cut costs [8].

In recent years, two-dimensional (2D) transition-metal dichalcogenides (TMDs) including MoS_2 [9], WS_2 [10], WSe_2 [11], $MoSe_2$ [12], etc., have emerged as competitive alternatives for HER to Pt-based electrocatalysts due to their numerous advantages, including excellent catalytic activity, high stability, and low costs [13]. Generally, the monolayer TMDs consist of a transition-metal atomic plane (Mo, W, Re, Hf, etc.) sandwiched between two chalcogen (S or Se) planes [14]. The adjacent layers of 2D TMDs are coupled by van der Waals force to construct bulk crystals [15]. Among them, nonprecious 2D $MoSe_2$ has received widespread attention as a promising HER catalyst due to its fascinating structures

and low Gibbs free energy [16]. However, it is well-known that the HER performance of 2D $MoSe_2$ is strongly limited by its weak conductivity and the lack of exposed active edges, which play key roles in the HER process [17–19]. At present, the two parameters are still challenging to simultaneously optimize. Furthermore, $MoSe_2$-based catalysts exhibit higher HER activity in acidic media, but often show slower HER kinetics in alkaline media because the HER activity under alkaline conditions is strongly limited by the lack of H^+. Hence, these above shortcomings result in its severely limited potential application in the HER.

To address these issues, combining 2D $MoSe_2$ with metallic TMDs such as $CoSe_2$ [20], $Ni_{0.85}Se$ [21], NiSe [22], $NiSe_2$ [23], etc., has been demonstrated as an effective strategy to promote its catalytic HER performance under alkaline conditions. For instance, Wang et al. reported that $MoSe_2$–$CoSe_2$ nanotubes present highly efficient performance for HER in the alkaline medium because their unique hierarchical architecture can suppress the restacking of $MoSe_2$ layers to gain more active sites for HER [24]. Zhou et al. found that the electrons in $MoSe_2$-NiSe nanohybrids can be easily transferred from the metallic NiSe nanocrystallite to the exposed $MoSe_2$ edges, thus enhancing HER performance [22]. Similarly, Zhang et al. demonstrated that 3D $MoSe_2$@$Ni_{0.85}Se$ nanowire exhibits remarkably improved alkaline HER performance because the conductive $Ni_{0.85}Se$ can facilitate fast electron transfers from the electrode to the exposed $MoSe_2$ edges [16]. Despite such great achievements that have been made, it is urgent to design and synthesize novel $MoSe_2$-based bimetallic selenides for further improving HER performance compared with noble metal-based catalysts.

In addition to this strategy, carbon-based materials such as MOF-derived carbon [25], carbon nanotube [26], graphene [27], etc., are broadly applied in enhancing the catalytic performance of transition-metal selenides. In particular, graphene has been demonstrated as an ideal carbon matrix for the transition-metal selenide catalysts, owing to its large surface area, adjustable porosity, high conductivity, and uniform catalyst distribution [28]. Considering the above, it is expected that a simple method can be developed to synthesize Mo-based bimetallic selenides incorporated with graphene as efficient hybrid electrocatalysts for HER under alkaline conditions.

In this work, we proposed a simple hydrothermal reaction to construct a $NiSe_2$-$MoSe_2$ heterostructures grown on graphene nanosheets ($NiSe_2$-$MoSe_2$ HTs/G). It demonstrated that the $NiSe_2$-$MoSe_2$ HTs constructed by metallic $NiSe_2$ nanocrystallites embedded in few-layer $MoSe_2$ nanosheets show a remarkably enhanced HER performance in alkaline media compared to pure $MoSe_2$ and $NiSe_2$. When supported on graphene, its HER performance can be further improved. The enhanced HER activity of $NiSe_2$-$MoSe_2$ HTs/G can be mainly attributed to the synergistic effects between metallic $NiSe_2$ nanocrystallites and $MoSe_2$ nanosheets, which can efficiently promote the rapid electron transfer from metallic $NiSe_2$ to the exposed $MoSe_2$ edges. Furthermore, the unique nanostructure of $NiSe_2$-$MoSe_2$ heterostructures supported on highly conductive graphene can not only efficiently expose the active sites on the heterostructures but also greatly enhance the overall conductivity of the composite, thus resulting in superior HER performance. This work might shed new light on the rational synthesis of graphene-supported bimetallic selenide heterostructures of the tunable HER activities.

2. Results and Discussion

$NiSe_2$-$MoSe_2$ heterostructures grown on graphene nanosheets ($NiSe_2$-$MoSe_2$ HTs/G) were synthesized by a one-step hydrothermal method. In the hydrothermal process, the graphene oxides (GO) were reduced to graphene nanosheets by hydrazine hydrate. Meanwhile, the Ni^{2+} and Mo^{4+} cations reacted with Se^{2-} anions to form $NiSe_2$-$MoSe_2$ heterostructures, which were in situ grown on reduced graphene nanosheets to obtain $NiSe_2$-$MoSe_2$ HTs/G composite. The crystalline structures of $NiSe_2$, $MoSe_2$, $NiSe_2$-$MoSe_2$ HTs, and $NiSe_2$-$MoSe_2$ HTs/G were determined by X-ray diffraction (XRD). The diffraction peaks at 13.25°, 31.78°, 37.98°, and 56.01° in the XRD pattern of $MoSe_2$ (Figure S1a) correspond to the (002), (100), (103), and (110) planes of hexagonal 2H-$MoSe_2$, respectively (JCPDS No. 87-2419). In the XRD patterns of $NiSe_2$ (Figure S1b), $NiSe_2$-$MoSe_2$ HTs, and

$NiSe_2$-$MoSe_2$ HTs/G (Figure 1a), the diffraction peaks at 29.95°, 33.58°, 36.89°, 42.86°, 50.74°, 55.52°, and 57.81° are ascribed to the (200), (210), (211), (220), (311), (023), and (321) planes of cubic $NiSe_2$, respectively (JCPDS No. 89-7161). It is worth noting that there are no obvious diffraction peaks of $MoSe_2$ appear in both $NiSe_2$-$MoSe_2$ HTs and $NiSe_2$-$MoSe_2$ HTs/G samples, suggesting the $MoSe_2$ in the composites with few layers or low crystallinity. This demonstrates that the formation of $NiSe_2$-$MoSe_2$ heterostructures can prevent the restacking of the adjacent layers for 2D $MoSe_2$. As shown in Raman profiles (Figure 1b), both $NiSe_2$-$MoSe_2$ HTs and $NiSe_2$-$MoSe_2$ HTs/G samples present bands that are identical with the characteristic peaks observed on pure $NiSe_2$ and $MoSe_2$ counterparts (Figure S2), implying the coexistence of $NiSe_2$ and 2H-$MoSe_2$ in these two composites. In detail, the band at 215.2 cm^{-1} is corresponded to the A_g signal of $NiSe_2$, while the bands at 238.1 and 287.6 cm^{-1} are associated with the A_{1g} and E^1_{2g} vibration modes of 2H-$MoSe_2$ [16]. Moreover, the D (1348.8 cm^{-1}) and G (1592.1 cm^{-1}) bands of graphene are observed in the Raman spectrum of $NiSe_2$-$MoSe_2$ HTs/G, which suggests the formation of the $NiSe_2$-$MoSe_2$ HTs/G hybrid [29]. The high I_D/I_G value (1.14) indicated that the reduced graphene has abundant carbon defects, which can efficiently promote the growth of $NiSe_2$-$MoSe_2$ heterostructures on the surfaces of graphene nanosheets [30].

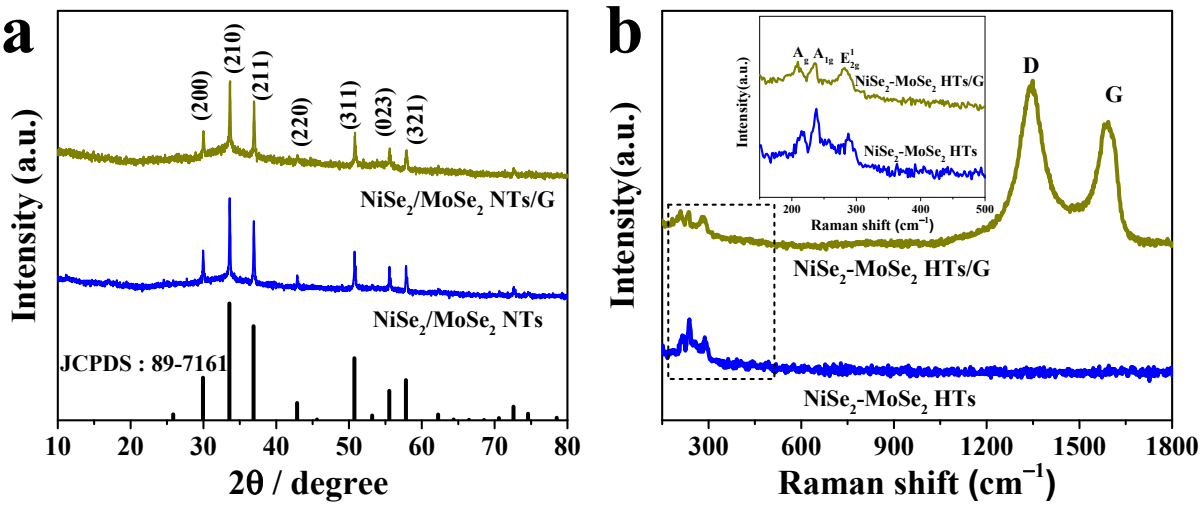

Figure 1. (**a**) XRD patterns of $NiSe_2$-$MoSe_2$ HTs and $NiSe_2$-$MoSe_2$ HTs/G composite. (**b**) Raman spectra of $NiSe_2$-$MoSe_2$ HTs and $NiSe_2$-$MoSe_2$ HTs/G composite. The inset is the enlarged Raman spectra.

The chemical states of as-prepared $NiSe_2$/$MoSe_2$ Hs/G composite were measured by X-ray photoelectron spectroscopy (XPS). As shown in Figure 2a, the predominant elements of Ni, Mo, Se, and C are observed in the XPS survey spectrum of the $NiSe_2$/$MoSe_2$ Hs/G composite. The Ni 2p spectrum (Figure 2b) demonstrates that peaks located at 853.6 and 870.9 eV are assigned to the Ni^0 $2p_{3/2}$ and Ni^0 $2p_{1/2}$ of metallic $NiSe_2$, and a couple of peaks located at 856.1 and 873.7 eV belong to the Ni^{2+} $2p_{3/2}$ and Ni^{2+} $2p_{1/2}$ of Ni oxidation state [31]. Moreover, the remaining two peaks located at 860.8 and 877.9 eV are ascribed to the satellite peaks of Ni 2p [32]. In the Mo 3d spectrum (Figure 2c), the Mo^{4+} $3d_{5/2}$ and Mo^{4+} $3d_{3/2}$ peaks are observed at 228.4 and 231.7 eV, which are ascribed to Mo^{4+} in $MoSe_2$ [33]. Furthermore, the relatively smaller peak at 230.1 eV is attributed to the Se 3s, while the high binding-energy peaks of Mo^{6+} $3d_{5/2}$ (232.7) and Mo^{6+} $3d_{3/2}$ (235.5 eV) correspond to MoO_3 species, which may result from the oxidation of the catalyst sample in air [24]. In the Se 3d spectrum (Figure 2d), the Se $3d_{5/2}$ and Se $3d_{3/2}$ peaks appear at 54.1 and 55.2 eV, respectively, revealing the existence of Se^{2-} [34]. In addition, another peak at 58.9 eV is originated from the oxidation states of the exposed Se edge [35]. The XPS data of Ni 2p, Mo 3d and Se 3d including peak positions and amounts for the composite material is summarized in Table S1. The ratio of Ni to Mo in the hybrid material is ~1.16:1, which is close to the raw materials. In the C 1s spectrum (Figure S3), the peaks located at

284.6, 286.7, and 288.9 eV are attributed to the C-C, C-O, and COOH bonds of graphene, respectively [36]. These XPS results further confirm that the $NiSe_2$-$MoSe_2$ HTs/graphene composite was successfully formed in the one-step hydrothermal process.

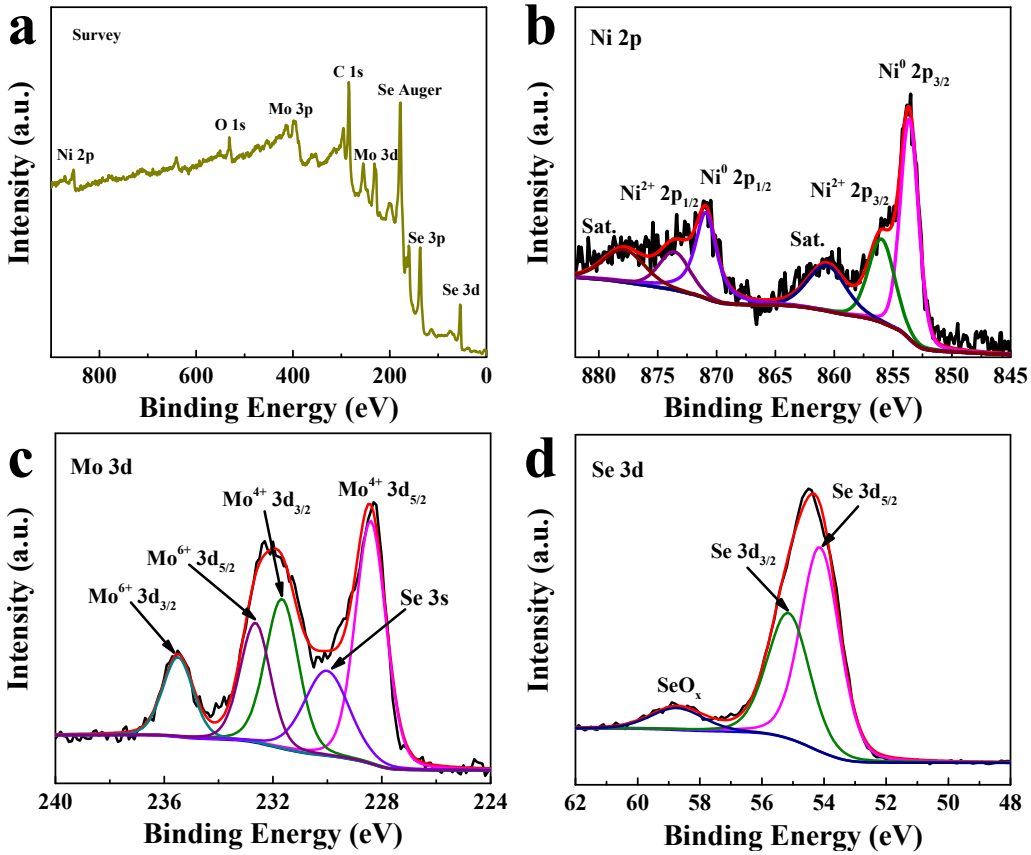

Figure 2. XPS spectra of $NiSe_2$-$MoSe_2$ HTs/G composite: (**a**) survey, (**b**) Ni 2p, (**c**) Mo 3d, and (**d**) Se 3d.

The morphologies of $MoSe_2$, $NiSe_2$, $NiSe_2$-$MoSe_2$ HTs, and $NiSe_2$-$MoSe_2$ HTs/G were first characterized by SEM. The SEM images shown in Figure S4 indicate that pure $MoSe_2$ has a flower-like morphology with many nanosheets. In sharp contrast, pure $NiSe_2$ presents large globular nanostructures with an average size of 100 nm (Figure S5). Notably, the $NiSe_2$-$MoSe_2$ HTs show a similar morphology with no obvious stack compared to pure $MoSe_2$ (Figure 3a). More importantly, there are no large globular $NiSe_2$ nanostructures that appear in the $NiSe_2$-$MoSe_2$ HTs (Figure 3b), which suggests that the $NiSe_2$-$MoSe_2$ heterostructures prevented the growing up of pure $NiSe_2$. As shown in Figure 3c, the $NiSe_2$-$MoSe_2$ HTs have been uniformly grown on the graphene matrix in the hydrothermal process because of the rich oxidizing functional groups on graphene oxide are beneficial to the growth of the catalysts [37]. Undoubtedly, the porous graphene matrixes with high conductivity can remarkably enhance the electron transfer from the electrode to the active sites on $NiSe_2$-$MoSe_2$ HTs and further improve the HER performance [38]. Furthermore, the high-resolution SEM image (Figure 3d) indicates that the graphene matrixes efficiently prevent the aggregation of $NiSe_2$-$MoSe_2$ HTs, thus promoting the maximumly exposed reactive sites.

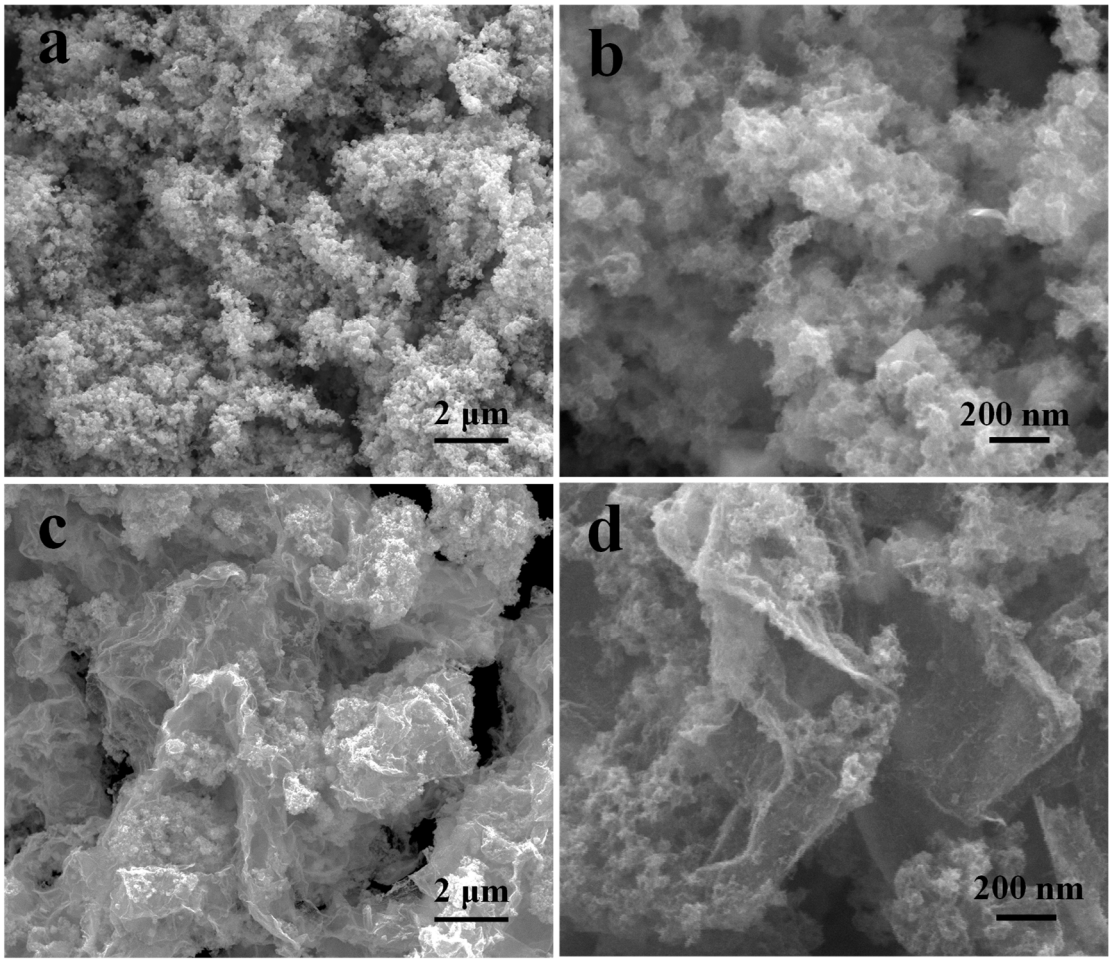

Figure 3. (**a**,**b**) SEM images of $NiSe_2$-$MoSe_2$ HTs. (**c**,**d**) SEM images of $NiSe_2$-$MoSe_2$ HTs/G composite.

The TEM analysis was further used to characterize the nanostructures of the $NiSe_2$-$MoSe_2$ HTs/G composite. The TEM images (Figure 4a,b) show that the uniform $NiSe_2$-$MoSe_2$ HTs nanostructures are tightly supported on the surfaces of graphene, which is consistent with SEM images. The high-resolution TEM image (Figure 4c) further indicates that many nanosheet-like $MoSe_2$ nanostructures present abundant exposed few-layered edges, implying that combining $MoSe_2$ with $NiSe_2$ and graphene can be advantageous to prevent the stack of $MoSe_2$ layers and maximally expose more active $MoSe_2$ edges. Moreover, the HRTEM images (Figures 4d and S6) demonstrate the formation of the $NiSe_2$-$MoSe_2$ heterostructures, which are constructed by $NiSe_2$ nanocrystallites uniformly embedded in few-layered $MoSe_2$ nanosheets (<10 layer). Compared to pure $NiSe_2$, the $NiSe_2$ nanocrystallites show a smaller particle size of ~10 nm. The discontinuous and distortion lattice fringes reveal that the $NiSe_2$ and $MoSe_2$ in the heterostructures possess rich defects, which can be employed as active sites in HER reaction [39]. Compared with bulk $MoSe_2$ (0.65 nm), the highly expanded lattice fringe of about 0.68 nm corresponds to the (002) planes of 2H-$MoSe_2$ [40]. The clear lattice fringes of 2H-$MoSe_2$ indicate that the $MoSe_2$ in the $NiSe_2$-$MoSe_2$ hybrid is not amorphous. In addition, the lattice fringes of 0.27 nm on ultra-small $NiSe_2$ nanocrystallites correspond to the (210) planes of cubic $NiSe_2$ [41]. The relevant element-mapping images of $NiSe_2$-$MoSe_2$ heterostructure-grown graphene (Figure 4e–h) display that the Ni, Mo, and Se elements are evenly distributed across the nanosheet-like nanostructure (Figure S7), suggesting that the ultra-small $NiSe_2$ nanoparticles are uniformly distributed in the $MoSe_2$ nanosheets.

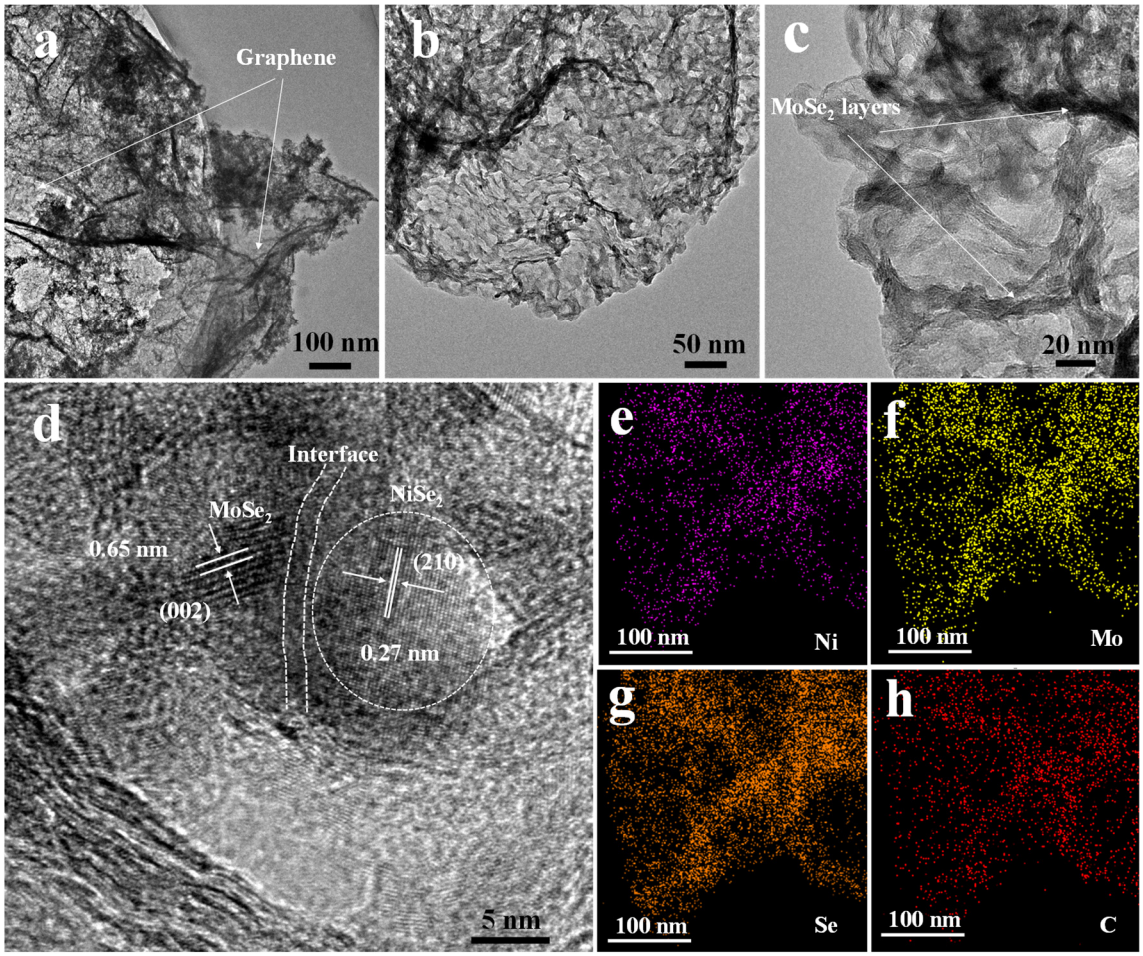

Figure 4. (**a**–**c**) TEM images of $NiSe_2$-$MoSe_2$ HTs/G composite. (**d**) High-resolution TEM (HRTEM) images of $NiSe_2$-$MoSe_2$ HTs/G. (**e**–**h**) EDS elemental mapping images of $NiSe_2$-$MoSe_2$ HTs/G.

The $NiSe_2$, $MoSe_2$, $NiSe_2$-$MoSe_2$ HTs, $NiSe_2$-$MoSe_2$ HTs/G, and Pt-C samples were used as HER catalysts to assess their electrocatalytic performance in 1.0 M KOH solution using the linear-sweep voltammetry measurement. Before tests, the electrolyte was bubbled with N_2 saturation for 30 min. As displayed in Figure 5a, the LSV curves indicate that the 20% Pt-C catalyst delivers the highest HER activity in 1.0 M KOH, which is consistent with the previous report [42]. Compared to pure $NiSe_2$ and $MoSe_2$, the $NiSe_2$-$MoSe_2$ HTs composite exhibits a remarkedly improved electrocatalytic performance. Since the pure $NiSe_2$ and $MoSe_2$ in our work show inferior electrocatalytic activity, the much-enhanced HER performance of $NiSe_2$-$MoSe_2$ HTs can be attributed to the synergistic effect of $NiSe_2$ nanocrystallites and $MoSe_2$ nanosheets. The metallic $NiSe_2$ nanocrystallites embedded in $MoSe_2$ nanosheets can boost the electrons' rapid transfer from the graphene matrix to the exposed $MoSe_2$ edges to take part in the HER reaction, and thus promoting the HER kinetics [43]. More importantly, the electrocatalytic HER performance of $NiSe_2$-$MoSe_2$ HTs/G is remarkably improved compared with $NiSe_2$-$MoSe_2$ HTs, which suggests that the adding of graphene further enhances their HER performance. It can be expected that the highly conductive graphene nanosheets can accelerate the electron transfers from the electrode to $NiSe_2$-$MoSe_2$ HTs, and therefore further promoting the HER kinetics. As a result, $NiSe_2$-$MoSe_2$ HTs/G delivers a much lower onset overpotential of 69 mV, compared with $NiSe_2$-$MoSe_2$ HTs (119 mV), $NiSe_2$ (164 mV), and $MoSe_2$ (196 mV). More importantly, a current density of 10 mA cm^{-2} was achieved at a relatively small overpotential of 144 mV, which is lower than that of $NiSe_2$-$MoSe_2$ HTs (212 mV), $NiSe_2$ (258 mV), and $MoSe_2$ (319 mV). In addition, $NiSe_2$-$MoSe_2$ HTs/G possesses favorable catalytic HER perfor-

mance compared to most of the TMDs-based HER electrocatalysts reported in recent years (Table S2), such as $CoSe_2$-$MoSe_2$/rGO-C (215 mV) [44], $MoSe_2$-NiSe@C heterostructures (154 mV) [33], 10% Ni–WSe_2 (215 mV) [45], $MoSe_2$–$CoSe_2$ NTs (206 mV) [24], $NiSe_2$/MoS_2 heterostructures (188 mV) [46], and so on, suggesting the potential practical application of $NiSe_2$-$MoSe_2$ HTs/G in alkaline electrolyte.

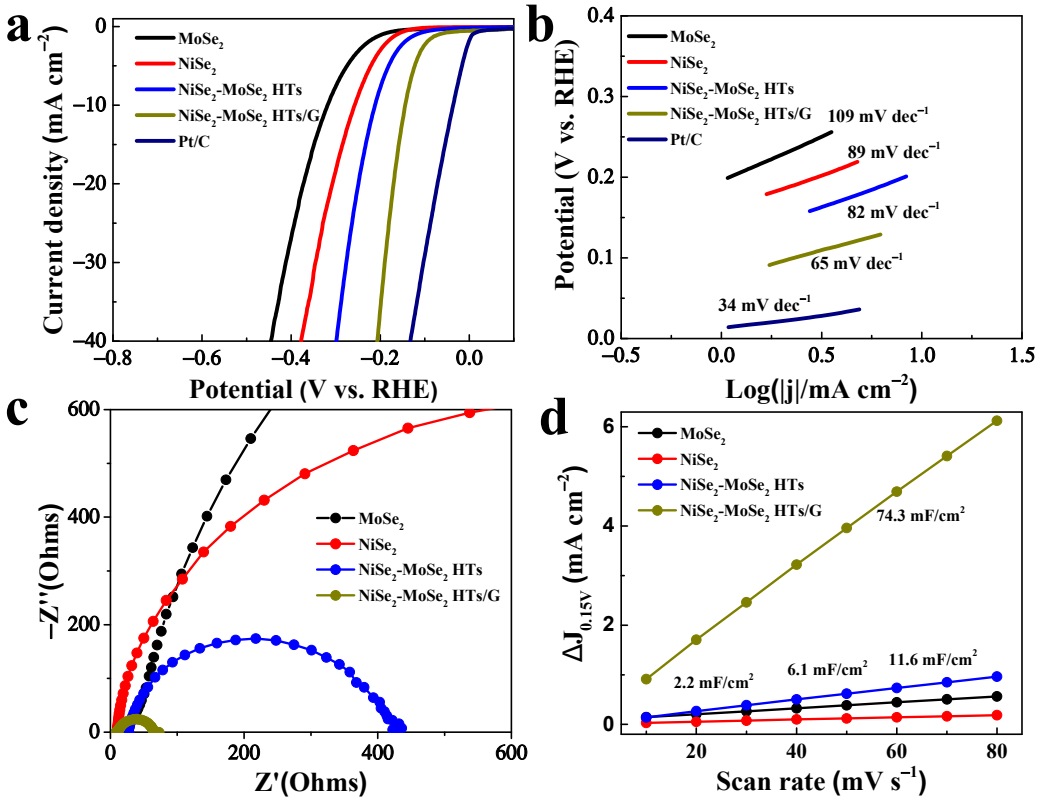

Figure 5. (**a**) Polarization curves of $MoSe_2$, $NiSe_2$, $NiSe_2$-$MoSe_2$ HTs, $NiSe_2$-$MoSe_2$ HTs/G, and Pt/C. (**b**) Tafel plots of $MoSe_2$, $NiSe_2$, $NiSe_2$-$MoSe_2$ HTs, $NiSe_2$-$MoSe_2$ HTs/G, and Pt/C. (**c**) EIS spectra of $MoSe_2$, $NiSe_2$, $NiSe_2$-$MoSe_2$ HTs, and $NiSe_2$-$MoSe_2$ HTs/G. (**d**) Estimated C_{dl} of $MoSe_2$, $NiSe_2$, $NiSe_2$-$MoSe_2$ HTs, and $NiSe_2$-$MoSe_2$ HTs/G.

As shown in Figure 5b, the HER kinetics of as-prepared catalysts were first investigated by Tafel plots. It is noted that the Tafel slope of $NiSe_2$-$MoSe_2$ HTs/G is 65 mV dec^{-1}, which is lower than those of 82 mV dec^{-1} for $NiSe_2$-$MoSe_2$ HTs hybrid, pure $NiSe_2$ for 89 mV dec^{-1}, pure $MoSe_2$ for 109 mV dec^{-1}, and close to the commercial Pt-C of 34 mV dec^{-1}, indicating the faster kinetics of $NiSe_2$-$MoSe_2$ HTs/G for HER in alkaline solution [47]. A smaller Tafel slope of 65 mV dec^{-1} for $NiSe_2$-$MoSe_2$ HTs/G suggests that the HER kinetics on this composite abides by the Volmer-Heyrovsky mechanism with the Heyrovsky step being rate-limiting in the alkaline HER process [48]. Furthermore, EIS measurement was employed to study the HER kinetics. The calculated charge-transfer resistance (R_{ct}) of $NiSe_2$-$MoSe_2$ HTs/G (Figure 5c) is 58.7 Ω, which is much lower than that of $NiSe_2$-$MoSe_2$ HTs (392.4 Ω), $NiSe_2$ (1462 Ω), and $MoSe_2$ (3764 Ω), demonstrating more rapid charge transfers within the composite [49]. According to these results, we can surmise that the faster HER kinetic in alkaline solution is attributed to the promoted charge transfer by metallic $NiSe_2$ and conductive graphene. In addition, the electrochemical active surface areas (ECSA) of $NiSe_2$-$MoSe_2$ HTs/G, $NiSe_2$-$MoSe_2$ HTs, pure $NiSe_2$, and pure $MoSe_2$ were assessed by extracting the electrochemical double-layer capacitances (C_{dl}) from their corresponding voltammograms (Figure S8) to obtain insight into catalytic active sites for HER. As shown in Figure 5d, a very large C_{dl} value (74.3 mF/cm^2) for $NiSe_2$-$MoSe_2$ HTs/G was achieved, which is much higher than those of 11.6 mF/cm^2 for $NiSe_2$-$MoSe_2$ HTs, 2.2 mF/cm^2 for pure $NiSe_2$, and 6.1 mF/cm^2 for pure $MoSe_2$, demonstrating the rich

electrocatalytic active sites in the composite. These abundant active sites can be attributed to the unique heterostructures supported on graphene that efficiently prevent the stack of the $MoSe_2$ layers and the aggregation of $NiSe_2$ [21].

To measure the stability of the as-prepared $NiSe_2$-$MoSe_2$ HTs/G composite during HER testing under alkaline conditions, a successive 3000 CV measurement was performed (Figure 6a). It indicated that the LSV curve shape of $NiSe_2$-$MoSe_2$ HTs/G after 3000 CV cycles is very close to the initial one, revealing the excellent stability under alkaline condition. Moreover, the HER stability of $NiSe_2$-$MoSe_2$ HTs/G was also evaluated by using a time dependence of the current density (i-t) test at a constant overpotential of 144 mV. As shown in Figure 6b, the current density at 10 mA cm^{-2} displays no significant variation from 0 to 24 h, suggesting the long-term stability in the alkaline HER.

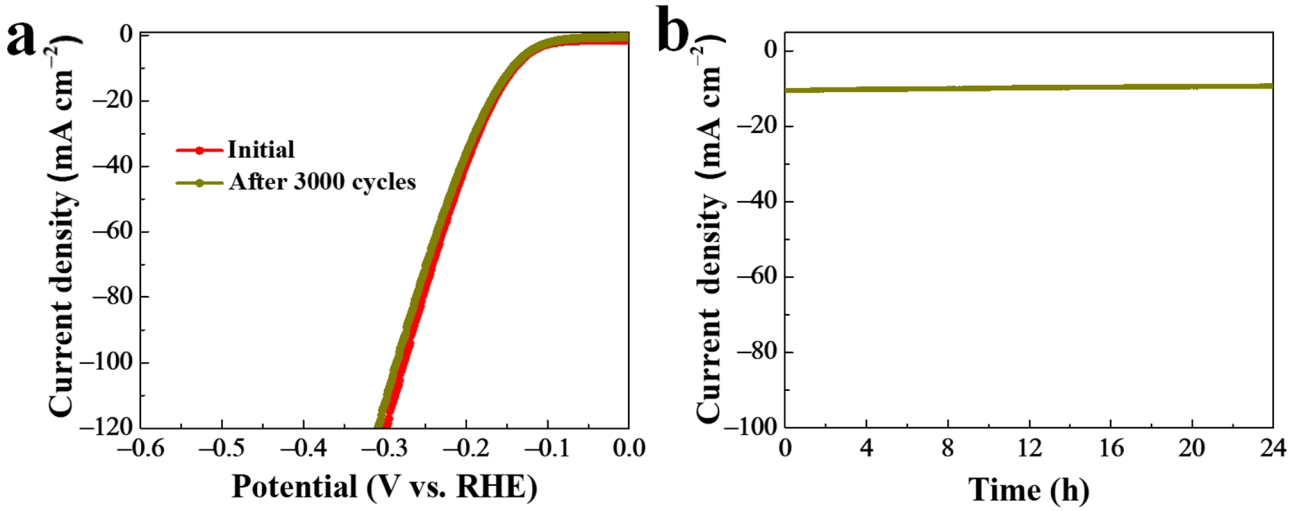

Figure 6. (**a**) Stability of $NiSe_2$-$MoSe_2$ HTs/G after 3000 CV tests. (**b**) I-t test of H-$NiSe_2$/$MoSe_2$/G under a constant overpotential of 144 mV.

3. Experimental Section

3.1. Synthesis of $NiSe_2$-$MoSe_2$ HTs/G

$NiSe_2$-$MoSe_2$ heterostructures grown on graphene nanosheets ($NiSe_2$-$MoSe_2$ HTs/G) were synthesized by a simple hydrothermal method. In a typical procedure, 8 mmol of Se powder was dispersed and slowly dissolved in 8 mL of hydrazine hydrate (HHA) to form a red solution A. Subsequently, 120 mg of GO powder was dispersed in 52 mL of distilled water, and then 2 mmol of nickel chloride hexahydrate ($NiCl_2 \cdot 6\ H_2O$) and 2 mmol of sodium molybdate tetrahydrate ($NaMoO_4 \cdot 4\ H_2O$) were successively dissolved in above dispersion to obtain solution B. Finally, solution A was slowly poured into the solution B under continuous stirring for 20 min and was carefully transferred into 100 mL of autoclave and then heated to the reaction temperature of 200 °C for 20 h. The as-obtained black precipitate was filtered from the solution and washed using distilled water and ethanol repeatedly. After drying at 60 °C, the above product was collected.

3.2. Synthesis of $NiSe_2$/$MoSe_2$ HTs

The synthetic procedure of $NiSe_2$/$MoSe_2$ HTs was the same as that of $NiSe_2$-$MoSe_2$ HTs/G without adding GO.

3.3. Synthesis of $NiSe_2$ or $MoSe_2$

The synthetic procedures of $NiSe_2$ or $MoSe_2$ were the same as that of $NiSe_2$/$MoSe_2$ HTs just using 4 mmol of $NiCl_2 \cdot 6\ H_2O$ or 4 mmol of $NaMoO_4 \cdot 4\ H_2O$ as metal sources, respectively.

3.4. Characterizations

X-ray diffraction (XRD) measurement (Rigaku D/MAX-rA, Rigaku, Tokyo, Japan) was conducted to obtain the crystallography of the as-synthesized samples. Raman spectroscopy (Horiba, Lille, France) with a 532 nm Argon laser, was used to determine the bonding nature of as-synthesized materials. The morphology and microstructure of as-obtained products were observed by a scanning electron microscope (SEM, FEI Inspect F50, Thermo Fisher Scientific, Waltham, USA) and transmission electron microscopy (TEM, FEIG2F20, Thermo Fisher Scientific, Waltham, USA). The surface chemistries and information of $NiSe_2$-$MoSe_2$ HTs/G were collected by X-ray photoelectron spectroscopy (XPS) equipped with Al Kα source (AXI Sultra DLD, Kratos, Manchester, UK).

3.5. Electrochemical Measurements

Electrochemical measurements were conducted using a CHI670E workstation. The HER catalytic activities of as-synthesized catalysts were evaluated by a three-electrode system in 1.0 M KOH solution. In this system, a Hg/HgO electrode was used as the reference electrode, and a graphite rod was used as the counter electrode. In this work, the working electrodes were prepared as follows. Firstly, 4 mg of the 20% Pt/C or as-prepared catalysts were mixed with 600 µL deionized water and 350 µL of absolute ethanol by sonication for 30 min. Subsequently, 50 µL of Nafion solution (5 wt%) was added into the former aqueous dispersion under continuing sonication for 10 min to form the catalyst ink. A droplet of the ink (10 µL) was dripped onto a working electrode (glassy carbon electrode, 3 mm diameter) and left to dry in natural conditions. For the activation, 30 cyclic voltammetry (CV) cycles should be performed at 100 mV s^{-1} from -0.7 to -1.4 V (vs. Hg/HgO) before all the tests. The polarization curves were carried out at a scan rate of 5 mV s^{-1}. We applied the EIS measurement to study the HER catalytic kinetics, which is measured at an overpotential of 150 mV vs. RHE with an AC voltage (5 mV amplitude, 0.1 Hz–100 kHz). The electrochemical double-layer capacitance (C_{dl}) was assessed by the CV tests in a potential range of 0.1–0.2 V vs. RHE with different scan rates (10–80 mV s^{-1}). The electrochemical stability in the HER process was investigated at a constant overpotential of 144 mV vs. RHE. All potentials in our work need to be switched to a reversible hydrogen electrode (RHE) by this equation ($E_{(RHE)} = E_{Hg/HgO} + 0.099 + 0.059 \times pH$).

4. Conclusions

In summary, $NiSe_2$-$MoSe_2$ heterostructures constructed by embedding metallic $NiSe_2$ nanocrystallites in few-layer $MoSe_2$ nanosheets have been supported on graphene nanosheets by a simple hydrothermal reaction. The metallic $NiSe_2$ and conductive graphene play key roles to enhance HER performance. The metallic $NiSe_2$ can prevent the restacking of $MoSe_2$ layers in the hydrothermal process to expose much more active edges. Furthermore, the graphene provides a conductive matrix for the growth of $NiSe_2$-$MoSe_2$ heterostructures, thus facilitating the fast electron transfers and HER kinetics. As a result, $NiSe_2$-$MoSe_2$ HTs/G composite exhibits a small overpotential of 144 mV at 10 mA cm^{-2}, a low Tafel slope of 65 mV dec^{-1}, and long-term stability for 24 h in alkaline media, which are comparable with most TMD-based catalysts (Table S2). The superior HER performance is ascribed to the unique $NiSe_2$-$MoSe_2$ heterostructures supported on graphene that can synergistically modulate the conductivity as well as exposed active sites. Our work provides a simple vision to synthesize graphene-supported bimetallic selenide heterostructures as highly efficient and stable electrocatalysts for HER.

Supplementary Materials: The following supporting information can be downloaded at: https://www.mdpi.com/article/10.3390/catal12070701/s1, Figure S1: XRD patterns of pure $MoSe_2$ and $NiSe_2$; Figure S2: Raman spectra of pure $MoSe_2$ and $NiSe_2$; Figure S3: XPS spectrum of C 1s for $NiSe_2$-$MoSe_2$ HTs/G; Figure S4: SEM images of pure $MoSe_2$; Figure S5: SEM images of pure $NiSe_2$; Figure S6: TEM image of $NiSe_2$-$MoSe_2$ HTs/G; Figure S7: STEM image and corresponding EDS elemental mapping area of $NiSe_2$-$MoSe_2$ HTs/G; Figure S8: Voltammogram of the different catalysts; Table S1:

XPS data including peak positions and amounts of $NiSe_2$-$MoSe_2$ HTs/G; Table S2: Comparison of electrochemical performances. References [50–66] are cited in the Supplementary Materials.

Author Contributions: Conceptualization, X.W. and Z.Z.; methodology, H.X.; software, T.D.; validation, X.W. and T.D.; formal analysis, Z.Z.; investigation, T.D.; resources, Z.Z. and Y.L.; data curation, H.X.; writing—original draft preparation, T.D.; writing—review and editing, X.W. and Z.Z.; visualization, Y.X.; supervision, X.W. and Z.Z.; project administration, Z.Z.; funding acquisition, Z.Z. All authors have read and agreed to the published version of the manuscript.

Funding: This research was supported by Discipline and Master's Site Construction Project of Guiyang University by Guiyang City Financial Support Guiyang University [2021-xk13], the Key field Foundation of GuiZhou Provincial Department of Education (No KY[2020]046), the Natural Science Research Project of the Education Department of Guizhou Province (Grant No. QJHKYZ[2020]089).

Data Availability Statement: All the relevant data used in this study have been provided in the form of figures and tables in the published article, and all data provided in the present manuscript are available to whom it may concern.

Conflicts of Interest: The authors declare no conflict of interest.

References

1. Seh, Z.W.; Kibsgaard, J.; Dickens, C.F.; Chorkendorff, I.; Nørskov, J.K.; Jaramillo, T.F. Combining theory and experiment in electrocatalysis: Insights into materials design. *Science* **2017**, *355*, eaad4998. [CrossRef] [PubMed]
2. Men, Y.; Tan, Y.; Li, P.; Cao, X.; Jia, S.; Wang, J.; Chen, S.; Luo, W. Tailoring the 3d-orbital electron filling degree of metal center to boost alkaline hydrogen evolution electrocatalysis. *Appl. Catal. B Environ.* **2021**, *284*, 119718. [CrossRef]
3. Yang, L.; Huang, L.; Yao, Y.; Jiao, L. In-situ construction of lattice-matching NiP_2/$NiSe_2$ heterointerfaces with electron redistribution for boosting overall water splitting. *Appl. Catal. B Environ.* **2021**, *282*, 119584. [CrossRef]
4. Mao, B.; Sun, P.; Jiang, Y.; Meng, T.; Guo, D.; Qin, J.; Cao, M. Identifying the Transfer Kinetics of Adsorbed Hydroxyl as a Descriptor of Alkaline Hydrogen Evolution Reaction. *Angew. Chem. Int. Ed.* **2020**, *59*, 15232–15237. [CrossRef]
5. Suen, N.; Hung, S.; Quan, Q.; Zhang, N.; Xu, Y.; Chen, H.M. Electrocatalysis for the oxygen evolution reaction: Recent development and future perspectives. *Chem. Soc. Rev.* **2017**, *46*, 337–365. [CrossRef]
6. Zhang, H.; Maijenburg, A.W.; Li, X.; Schweizer, S.L.; Wehrspohn, R.B. Bifunctional Heterostructured Transition Metal Phosphides for Efficient Electrochemical Water Splitting. *Adv. Funct. Mater.* **2020**, *30*, 2003261. [CrossRef]
7. Xie, C.; Chen, W.; Du, S.; Yan, D.; Zhang, Y.; Chen, J.; Liu, B.; Wang, S. In-situ phase transition of WO_3 boosting electron and hydrogen transfer for enhancing hydrogen evolution on Pt. *Nano Energy* **2020**, *71*, 104653. [CrossRef]
8. Zhang, Y.; Ouyang, B.; Xu, J.; Chen, S.; Rawat, R.S.; Fan, H.J. 3D Porous Hierarchical Nickel-Molybdenum Nitrides Synthesized by RF Plasma as Highly Active and Stable Hydrogen-Evolution-Reaction Electrocatalysts. *Adv. Energy Mater.* **2016**, *6*, 1600221. [CrossRef]
9. Kibsgaard, J.; Chen, Z.; Reinecke, B.N.; Jaramillo, T. Engineering the surface structure of MoS_2 to preferentially expose active edge sites for electrocatalysis. *Nat. Mater.* **2012**, *11*, 963–969. [CrossRef]
10. Wang, H.; Xu, Z.; Zhang, Z.; Hu, S.; Ma, M.; Zhang, Z.; Zhou, W.; Liu, H. Addressable surface engineering for N-doped WS_2 nanosheet arrays with abundant active sites and the optimal local electronic structure for enhanced hydrogen evolution reaction. *Nanoscale* **2020**, *12*, 22541–22550. [CrossRef]
11. Wang, H.; Kong, D.; Johanes, P.; Cha, J.J.; Zheng, G.; Yan, K.; Liu, N.; Cui, Y. $MoSe_2$ and WSe_2 Nanofilms with Vertically Aligned Molecular Layers on Curved and Rough Surfaces. *Nano Lett.* **2013**, *13*, 3426–3433. [CrossRef] [PubMed]
12. Kwon, I.S.; Kwak, I.H.; Debela, T.T.; Abbas, H.G.; Park, Y.C.; Ahn, J.-P.; Park, J.; Kang, H.S. Se-Rich $MoSe_2$ Nanosheets and Their Superior Electrocatalytic Performance for Hydrogen Evolution Reaction. *ACS Nano* **2020**, *14*, 6295–6304. [CrossRef] [PubMed]
13. Lin, L.; Sherrell, P.; Liu, Y.; Lei, W.; Zhang, S.; Zhang, H.; Wallace, G.G.; Chen, J. Engineered 2D Transition Metal Dichalcogenides-A Vision of Viable Hydrogen Evolution Reaction Catalysis. *Adv. Energy Mater.* **2020**, *10*, 1903870. [CrossRef]
14. Zhang, X.; Lai, Z.; Ma, Q.; Zhang, H. Novel structured transition metal dichalcogenide nanosheets. *Chem. Soc. Rev.* **2018**, *47*, 3301–3338. [CrossRef]
15. Kwon, I.S.; Kwak, I.H.; Ju, S.; Kang, S.; Han, S.; Park, Y.C.; Park, J.; Park, J. Adatom Doping of Transition Metals in $ReSe_2$ Nanosheets for Enhanced Electrocatalytic Hydrogen Evolution Reaction. *ACS Nano* **2020**, *14*, 12184–12194. [CrossRef]
16. Zhang, L.; Wang, T.; Sun, L.; Sun, Y.; Hu, T.; Xu, K.; Ma, F. Hydrothermal synthesis of 3D hierarchical $MoSe_2$/$NiSe_2$ composite nanowires on carbon fiber paper and their enhanced electrocatalytic activity for the hydrogen evolution reaction. *J. Mater. Chem. A* **2017**, *5*, 19752–19759. [CrossRef]
17. Najafi, L.; Bellani, S.; Oropesa-Nuñez, R.; Prato, M.; Martín-García, B.; Brescia, R.; Bonaccorso, F. Carbon Nanotube-Supported $MoSe_2$ Holey Flake:Mo_2C Ball Hybrids for Bifunctional pH-Universal Water Splitting. *ACS Nano* **2019**, *13*, 3162–3176. [CrossRef]

18. Tan, C.; Luo, Z.; Chaturvedi, A.; Cai, Y.; Du, Y.; Gong, Y.; Huang, Y.; Lai, Z.; Zhang, X.; Zheng, L.; et al. Preparation of High-Percentage 1T-Phase Transition Metal Dichalcogenide Nanodots for Electrochemical Hydrogen Evolution. *Adv. Mater.* **2018**, *30*, 1705509. [CrossRef]
19. Jian, C.; Hong, W.; Cai, Q.; Liu, W. The local electronic structure modulation of the molybdenum selenide–nitride heterojunction for efficient hydrogen evolution reaction. *J. Mater. Chem. A* **2021**, *9*, 26113–26118. [CrossRef]
20. Zhao, G.; Li, P.; Rui, K.; Chen, Y.; Dou, S.X.; Sun, W. $CoSe_2$/$MoSe_2$ Heterostructures with Enriched Water Adsorption/Dissociation Sites towards Enhanced Alkaline Hydrogen Evolution Reaction. *Chem. Eur. J.* **2018**, *24*, 11158–11165. [CrossRef]
21. Wang, C.; Zhang, P.; Lei, J.; Dong, W.; Wang, J. Integrated 3D $MoSe_2$@$Ni_{0.85}Se$ Nanowire Network with Synergistic Cooperation as Highly Efficient Electrocatalysts for Hydrogen Evolution Reaction in Alkaline Medium. *Electrochim. Acta* **2017**, *246*, 712–719. [CrossRef]
22. Zhou, X.; Liu, Y.; Ju, H.; Pan, B.; Zhu, J.; Ding, T.; Wang, C.; Yang, Q. Design and Epitaxial Growth of $MoSe_2$–NiSe Vertical Heteronanostructures with Electronic Modulation for Enhanced Hydrogen Evolution Reaction. *Chem. Mater.* **2016**, *28*, 1838–1846. [CrossRef]
23. Qin, R.; Wang, P.; Li, Z.; Zhu, J.; Cao, F.; Xu, H.; Ma, Q.; Zhang, J.; Yu, J.; Mu, S. Ru-Incorporated Nickel Diselenide Nanosheet Arrays with Accelerated Adsorption Kinetics toward Overall Water Splitting. *Small* **2022**, *18*, 2105305. [CrossRef] [PubMed]
24. Wang, X.; Zheng, B.; Yu, B.; Wang, B.; Hou, W.; Zhang, W.; Chen, Y. In situ synthesis of hierarchical $MoSe_2$-$CoSe_2$ nanotubes as an efficient electrocatalyst for the hydrogen evolution reaction in both acidic and alkaline media. *J. Mater. Chem. A* **2018**, *6*, 7842–7850. [CrossRef]
25. Lu, H.; Zhang, Y.; Huang, Y.; Zhang, C.; Liu, T. Reaction Packaging $CoSe_2$ Nanoparticles in N-Doped Carbon Polyhedra with Bifunctionality for Overall Water Splitting. *ACS Appl. Mater. Interfaces* **2018**, *11*, 3372–3381. [CrossRef]
26. Zhang, M.; Hu, A.; Liu, Z.; Xu, Y.; Fan, B.; Tang, Q.; Zhang, S.; Deng, W.; Chen, X. Synergistic effect of three-dimensional cobalt diselenide/carbon nanotube arrays composites for enhanced hydrogen evolution reaction. *Electrochim. Acta* **2018**, *285*, 254–261. [CrossRef]
27. Mao, S.; Wen, Z.; Ci, S.; Guo, X.; Ostrikov, K.K.; Chen, J. Perpendicularly Oriented $MoSe_2$/Graphene Nanosheets as Advanced Electrocatalysts for Hydrogen Evolution. *Small* **2015**, *11*, 414–419. [CrossRef]
28. Chia, X.; Pumera, M. Characteristics and performance of two-dimensional materials for electrocatalysis. *Nat. Catal.* **2018**, *1*, 909–921. [CrossRef]
29. Yi, Y.; Sun, Z.; Li, C.; Tian, Z.; Lu, C.; Shao, Y.; Li, J.; Sun, J.; Liu, Z. Designing 3D Biomorphic Nitrogen-Doped $MoSe_2$/Graphene Composites toward High-Performance Potassium-Ion Capacitors. *Adv. Funct. Mater.* **2019**, *30*, 1903878. [CrossRef]
30. Wang, X.; He, J.; Yu, B.; Sun, B.; Yang, D.; Zhang, X.; Zhang, Q.; Zhang, W.; Gu, L.; Chen, Y. $CoSe_2$ nanoparticles embedded MOF-derived Co-N-C nanoflake arrays as efficient and stable electrocatalyst for hydrogen evolution reaction. *Appl. Catal. B Environ.* **2019**, *258*, 117996. [CrossRef]
31. Yang, Y.; Zhang, W.; Xiao, Y.; Shi, Z.; Cao, X.; Tang, Y.; Gao, Q. $CoNiSe_2$ heteronanorods decorated with lay-ered-double-hydroxides for efficient hydrogen evolution. *Appl. Catal. B Environ.* **2019**, *242*, 132–139. [CrossRef]
32. Hao, T.; Liu, Y.; Liu, G.; Peng, C.; Chen, B.; Feng, Y.; Ru, J.; Yang, J. Insight into faradaic mechanism of polyaniline@$NiSe_2$ core-shell nanotubes in high-performance supercapacitors. *Energy Storage Mater.* **2019**, *23*, 225–232. [CrossRef]
33. Liu, C.; Wang, K.; Zheng, X.; Liu, X.; Liang, Q.; Chen, Z. Rational design of $MoSe_2$-NiSe@carbon heteronanostructures for efficient electrocatalytic hydrogen evolution in both acidic and alkaline media. *Carbon* **2018**, *139*, 1–9. [CrossRef]
34. Zhang, X.; Zhang, Y.; Zhang, Y.; Jiang, W.; Zhang, Q.; Yang, Y.; Gu, L.; Hu, J.; Wan, L. Phase-Controlled Synthesis of 1T-$MoSe_2$/NiSe Heterostructure Nanowire Arrays via Electronic Injection for Synergistically Enhanced Hydrogen Evolution. *Small Methods* **2019**, *3*, 1800317. [CrossRef]
35. Wang, G.; Chen, W.; Chen, G.; Huang, J.; Song, C.; Chen, D.; Du, Y.; Li, C.; Ostrikov, K.K. Trimetallic Mo–Ni–Co selenides nanorod electrocatalysts for highly-efficient and ultra-stable hydrogen evolution. *Nano Energy* **2020**, *71*, 104637. [CrossRef]
36. Zhang, Y.; Yang, J.; Dong, Q.; Geng, H.; Zheng, Y.; Liu, Y.; Wang, W.; Li, C.C.; Dong, X. Highly Dispersive MoP Nanoparticles Anchored on Reduced Graphene Oxide Nanosheets for an Efficient Hydrogen Evolution Reaction Electrocatalyst. *ACS Appl. Mater. Interfaces* **2018**, *10*, 26258–26263. [CrossRef]
37. Wang, X.; Chen, Y.; Zheng, B.; Qi, F.; He, J.; Li, P.; Zhang, W. Few-layered WSe_2 nanoflowers anchored on graphene nanosheets: A highly efficient and stable electrocatalyst for hydrogen evolution. *Electrochim. Acta* **2016**, *222*, 1293–1299. [CrossRef]
38. Zhang, L.; Sun, L.; Huang, Y.; Sun, Y.; Hu, T.; Xu, K.; Ma, F. Hydrothermal synthesis of N-doped RGO/$MoSe_2$ composites and enhanced electro-catalytic hydrogen evolution. *J. Mater. Sci.* **2017**, *52*, 13561–13571. [CrossRef]
39. Kuang, P.; Tong, T.; Fan, K.; Yu, J. In Situ Fabrication of Ni-Mo Bimetal Sulfide Hybrid as an Efficient Electrocatalyst for Hy-drogen Evolution over a Wide pH Range. *ACS Catal.* **2017**, *7*, 6179–6187. [CrossRef]
40. Wu, M.; Huang, Y.; Cheng, X.; Geng, X.; Tang, Q.; You, Y.; Yu, Y.; Zhou, R.; Xu, J. Arrays of ZnSe/$MoSe_2$ Nanotubes with Electronic Modulation as Efficient Electrocatalysts for Hydrogen Evolution Reaction. *Adv. Mater. Interfaces* **2017**, *4*, 1700948. [CrossRef]
41. Sun, Y.; Xu, K.; Wei, Z.; Li, H.; Zhang, T.; Li, X.; Cai, W.; Ma, J.; Fan, H.J.; Li, Y. Strong Electronic Interaction in Du-al-Cation-Incorporated $NiSe_2$ Nanosheets with Lattice Distortion for Highly Efficient Overall Water Splitting. *Adv. Mater.* **2018**, *30*, 1802121. [CrossRef] [PubMed]

42. Bao, X.; Gong, Y.; Chen, Y.; Zhang, H.; Wang, Z.; Mao, S.; Xie, L.; Jiang, Z.; Wang, Y. Carbon vacancy defect-activated Pt cluster for hydrogen generation. *J. Mater. Chem. A* **2019**, *7*, 15364–15370. [CrossRef]
43. Zhu, M.; Yan, Q.; Xue, Y.; Yan, Y.; Zhu, K.; Ye, K.; Yan, J.; Cao, D.; Xie, H.; Wang, G. Free-Standing P-Doped $NiSe_2$/$MoSe_2$ Catalyst for Efficient Hydrogen Evolution in Acidic and Alkaline Media. *ACS Sustain. Chem. Eng.* **2022**, *10*, 279–287. [CrossRef]
44. Wang, B.; Wang, Z.; Wang, X.; Zheng, B.; Zhang, W.; Chen, Y. Scalable synthesis of porous hollow $CoSe_2$-$MoSe_2$/carbon microspheres for highly efficient hydrogen evolution reaction in acidic and alkaline media. *J. Mater. Chem. A* **2018**, *6*, 12701–12707. [CrossRef]
45. Kadam, S.R.; Enyashin, A.N.; Houben, L.; Bar-Ziv, R.; Bar-Sadan, M. Ni-WSe_2 nanostructures as efficient catalysts for electrochemical hydrogen evolution reaction (HER) in acidic and alkaline media. *J. Mater. Chem. A* **2020**, *8*, 1403–1416. [CrossRef]
46. Long, A.; Li, W.; Zhou, M.; Gao, W.; Liu, B.; Wei, J.; Zhang, X.; Liu, H.; Liu, Y.; Zeng, X. MoS_2 nanosheets grown on nickel chalcogenides: Controllable synthesis and electrocatalytic origins for the hydrogen evolution reaction in alkaline solution. *J. Mater. Chem. A* **2019**, *7*, 21514–21522. [CrossRef]
47. Men, Y.; Li, P.; Zhou, J.; Cheng, G.; Chen, S.; Luo, W. Tailoring the Electronic Structure of Co_2P by N Doping for Boosting Hydrogen Evolution Reaction at All pH Values. *ACS Catal.* **2019**, *9*, 3744–3752. [CrossRef]
48. Anjum, M.A.R.; Okyay, M.S.; Kim, M.; Lee, M.H.; Park, N.; Lee, J.S. Bifunctional sulfur-doped cobalt phosphide electrocat-alyst outperforms all-noble-metal electrocatalysts in alkaline electrolyzer for overall water splitting. *Nano Energy* **2018**, *53*, 286–295. [CrossRef]
49. Zhang, S.; Zhai, D.; Sun, T.; Han, A.; Zhai, Y.; Cheong, W.; Liu, Y.; Su, C.; Wang, D.; Li, Y. In situ embedding Co_9S_8 into nitrogen and sulfur codoped hollow porous carbon as a bifunctional electrocatalyst for oxygen reduction and hydrogen evolution reactions. *Appl. Catal. B Environ.* **2019**, *254*, 186–193. [CrossRef]
50. Maity, S.; Das, B.; Samanta, M.; Das, B.K.; Ghosh, S.; Chattopadhyay, K.K. $MoSe_2$-Amorphous CNT Hierarchical Hybrid Core–Shell Structure for Efficient Hydrogen Evolution Reaction. *ACS Appl. Energy Mater.* **2020**, *3*, 5067–5076. [CrossRef]
51. Truong, Q.D.; Nakayasu, Y.; Nguyen, Q.T.; Nguyen, D.N.; Nguyen, C.T.; Devaraju, M.K.; Rangappa, D.; Nayuki, K.; Sasaki, Y.; Tran, P.D.; et al. Defect-rich exfoliated $MoSe_2$ nanosheets by supercritical fluid process as an attractive catalyst for hydrogen evolution in water. *Appl. Surf. Sci.* **2020**, *505*, 144537. [CrossRef]
52. Zimron, O.; Zilberman, T.; Kadam, S.R.; Ghosh, S.; Kolatker, S.; Neyman, A.; Bar-Ziv, R.; Bar-Sadan, M. Co-Doped $MoSe_2$ Nanoflowers as Efficient Catalysts for Electrochemical Hydrogen Evolution Reaction (HER) in Acidic and Alkaline Media. *Isr. J. Chem.* **2020**, *60*, 624–629. [CrossRef]
53. Yin, Y.; Zhang, Y.; Gao, T.; Yao, T.; Zhang, X.; Han, J.; Wang, X.; Zhang, Z.; Xu, P.; Zhang, P.; et al. Synergistic Phase and Disorder Engineering in 1T-$MoSe_2$ Nanosheets for Enhanced Hydrogen-Evolution Reaction. *Adv. Mater.* **2017**, *29*, 1700311. [CrossRef] [PubMed]
54. Zhang, J.; Wu, M.; Shi, Z.; Jiang, M.; Jian, W.; Xiao, Z.; Li, J.; Lee, C.; Xu, J. Composition and Interface Engineering of Alloyed $MoS_{2x}Se_{2(1-x)}$ Nanotubes for Enhanced Hydrogen Evolution Reaction Activity. *Small* **2016**, *12*, 4379–4385. [CrossRef] [PubMed]
55. OMeiron, E.; Kuraganti, V.; Hod, I.; Bar-Ziv, R.; Bar-Sadan, M. Improved catalytic activity of $Mo_{1-x}W_xSe_2$ alloy nanoflowers promotes efficient hydrogen evolution reaction in both acidic and alkaline aqueous solutions. *Nanoscale* **2017**, *9*, 13998–14005. [CrossRef]
56. Qu, B.; Li, C.; Zhu, C.; Wang, S.; Zhang, X.; Chen, Y. Growth of $MoSe_2$nanosheets with small size and expanded spaces of (002) plane on the surfaces of porous N-doped carbon nanotubes for hydrogen production. *Nanoscale* **2016**, *8*, 16886–16893. [CrossRef]
57. Wang, R.; Han, J.; Xu, P.; Gao, T.; Zhong, J.; Wang, X.; Zhang, X.; Li, Z.; Xu, L.; Song, B. Dual-Enhanced Doping in $ReSe_2$ for Effi-ciently Photoenhanced Hydrogen Evolution Reaction. *Adv. Sci.* **2020**, *7*, 2000216. [CrossRef]
58. Qu, B.; Yu, X.; Chen, Y.; Zhu, C.; Li, C.; Yin, Z.; Zhang, X. Ultrathin $MoSe_2$ Nanosheets Decorated on Carbon Fiber Cloth as Binder-Free and High-Performance Electrocatalyst for Hydrogen Evolution. *ACS Appl. Mater. Interfaces* **2015**, *7*, 14170–14175. [CrossRef]
59. Chen, X.; Liu, G.; Zheng, W.; Feng, W.; Cao, W.; Hu, W.; Hu, P. Vertical 2D MoO_2/$MoSe_2$ Core-Shell Nanosheet Arrays as High-Performance Electrocatalysts for Hydrogen Evolution Reaction. *Adv. Funct. Mater.* **2016**, *26*, 8537–8544. [CrossRef]
60. Lin, H.; Li, H.; Li, Y.; Liu, J.; Wang, X.; Wang, L. Hierarchical CoS/MoS_2 and Co_3S_4/MoS_2/Ni_2P nanotubes for efficient electro-catalytic hydrogen evolution in alkaline media. *J. Mater. Chem. A* **2017**, *5*, 25410–25419. [CrossRef]
61. Chouki, T.; Donkova, B.; Aktarla, B.; Stefanov, P.; Emin, S. Growth of $MoSe_2$ electrocatalyst from metallic molybdenum nanoparticles for efficient hydrogen evolution. *Mater. Today Commun.* **2021**, *26*, 101976. [CrossRef]
62. Poorahong, S.; Somnin, C.; Mahamadou, I.M.; Dubois, C.; Chergui, S.; Peng, Z.; Su, Y.; Tran, T.X.; Thammakhet-Buranachai, C.; Mazzah, A.; et al. Nanoporous Graphite-like Membranes Decorated with $MoSe_2$ Nanosheets for Hydrogen Evolution. *ACS Appl. Nano Mater.* **2022**, *5*, 2769–2778. [CrossRef]
63. Shi, H.; Zhang, H.; Li, M.; Wang, Y.; Wang, D. Nanoflower-like 1T/2H mixed-phase $MoSe_2$ as an efficient elec-trocatalyst for hydrogen evolution. *J. Alloys Compd.* **2021**, *878*, 160381. [CrossRef]
64. Zhang, Y.; Zhang, S.; He, Y.; Li, H.; He, T.; Shi, H.; Ma, X.; Yang, Q.; Chen, L.; Chen, J. Self-supporting $MoSe_2$/$CoSe_2$@CFP electrocatalyst electrode for high-efficiency HER under alkaline solution. *J. Solid State Chem.* **2021**, *298*, 122108. [CrossRef]

65. Yang, B.; Huang, Z.; Wu, H.; Hu, H.; Lin, H.; Nie, M.; Li, Q. Sea urchin-like $CoSe_2$ nanoparticles modified graphene oxide as an efficient and stable hydrogen evolution catalyst. *J. Electroanal. Chem.* **2022**, *907*, 116037. [CrossRef]
66. Li, G.; Feng, S.; Wang, C.; Deng, P.; Li, J. Co-$NiSe_2$/NF nanosheet for efficient hydrogen evolution reaction. *Catal. Commun.* **2022**, *165*, 106443. [CrossRef]